JOURNAL OF APPLIED ELECTROCHEMISTRY 26 (1996) 785–793

Synthesis and characterization of Pt–Ti_4O_7 microelectrode arrays

L. HE, H. F. FRANZEN, D. C. JOHNSON

Department of Chemistry and Ames Laboratory, Iowa State University, Ames, Iowa 50011, USA

Received 21 July 1995

The synthesis of Pt–Ti_4O_7 microelectrode arrays is achieved from mixtures of TiO_2 and Ti_2O_3 powders plus Pt particles by a thermal procedure commonly used in solid-state chemistry. Data obtained for the Pt–Ti_4O_7 materials by X-ray diffractometry and scanning electron microscopy are consistent with the existence of heterogeneous mixtures of Pt particles imbedded within the conductive Ti_4O_7 matrices. Rotated disc electrodes (RDEs) constructed from pure Pt and from the Pt–Ti_4O_7 materials are compared on the basis of their voltammetric and amperometric response for I^- and H_2O_2 in 0.10 M H_2SO_4. The observed enhancement of current densities for the Pt–Ti_4O_7 RDEs is rationalized on the basis of the behaviour expected for microelectrode arrays.

1. Introduction

The search for inexpensive yet efficient electrode materials represents a major challenge to the advancement of electrolytic processes on the industrial scale. Platinum is a desirable electrode material for numerous potentially important industrial processes; however, the cost of this metal can be prohibitive in many applications. Because a suitable replacement for platinum has not been found, an attractive alternative to the use of solid platinum electrodes is the use of platinum microelectrode arrays at which current densities for desired processes, calculated relative to the active area, can be significantly higher than for the pure metal electrodes.

Conventionally, microelectrode arrays have consisted of ordered or random arrangements of conducting regions, typically microscale in dimension, separated from one another by a nonconductive binder (e.g., Kel-F) to hold the microelectrode particles into physically stable arrangements [1–3]. However, to achieve the optimal fractional active area of about, or less than 1.7%, as suggested by Weber for microelectrode arrays [4], it has been necessary to incorporate graphite particles within the plastic matrices to achieve electrical connectivity between the microelectrodes. In a recent study of these so-called 'Kelgraf electrodes' containing small Au particles [3], current densities were more than 10 times larger in comparison to those for the same reaction at pure Au electrodes of large geometry. However, two major disadvantages were recognized when using graphitic powder in the fabrication of these composite electrodes [3]. First, loss of graphite occurred at the surface when the composite materials were subjected to mechanical polishing. Hence, it is apparent that some metal particles can be lost and there can be a sacrifice in electrical connectivity between the remaining metal particles. Second, graphite is a reactive electrode material for many faradaic reactions and, therefore, its use can be undesirable in the fabrication of metal microelectrode arrays, especially when the products differ for reactions at the graphitic and metallic surfaces.

Significant advantages can result from fabrication of microelectrode arrays using matrices (binders) that are both electrically conductive and electrochemically inert. An excellent example of such a material is Ti_4O_7 which has previously been used for making Ru microelectrode arrays [5]. The Ti_4O_7 is one of the Magneli phases (Ti_nO_{2n-1}) which is a good conductor ($\sim 10^3\ \Omega^{-1}\,cm^{-1}$) and is very stable in a variety of corrosive media [6, 7]. Furthermore, the desired electrochemical inertness of Ti_4O_7 is indicated by large values of overpotential for anodic and cathodic evolution of oxygen and hydrogen, respectively, in aqueous media [6, 7]. Possible applications of Ti_4O_7 in electrolytic processes have been described in reviews [6, 7] and patents [8, 9].

In previous work, a significant enhancement in current density was observed for Ru–Ti_4O_7 RDEs in comparison to solid Ru RDE [5]. More specifically, relative current densities of 23 and 20 were obtained for the oxidation of I^- to I_2 and to IO_3^-, respectively, corresponding to a rotational velocity of 10.5 rad s^{-1} and a fractional active surface area of 1%. Here we report on efforts to generate arrays of platinum microelectrodes within conductive Ti_4O_7 matrices. X-ray diffraction and scanning electron micrographic data are presented along with voltammetric and amperometric results for the oxidations of I^- to I_2 and H_2O_2 to O_2 in 0.10 M H_2SO_4.

The amperometric response of microelectrode arrays can be characterized by the relative current density, J, defined as the true current density at the collective microelectrodes of the array normalized

0021-891X

with respect to the current density at a solid electrode of large geometry [3]:

$$J = \frac{(i/A_{act})_{array}}{(i/A_{geom})_{solid}} \quad (1)$$

The amperometric response at microelectrode arrays also has been characterized by a so-called 'attenuation factor', ρ, defined as the apparent current density at the array normalized with respect to the current density for a solid electrode of large geometry:

$$\rho = \frac{(i/A_{geom})_{array}}{(i/A_{geom})_{solid}} \quad (2)$$

Hence, from Equations 1 and 2, values of J and ρ are related according to

$$\frac{\rho}{J} = \frac{A_{act}}{A_{geom}} = 1 - \theta \quad (3)$$

where θ is a so-called 'blocking factor' [10–12] by analogy with partially fouled electrodes.

The effect of changes in rotational velocity, ω, for disc electrodes consisting of microelectrode arrays can be predicted easily for two limiting conditions. For low density arrays ($\theta \rightarrow 1$) with active sites that behave as isolated and ideal microelectrodes, current is expected to be independent of ω. However, because the transport-limited current at a solid RDE is proportional to $\omega^{1/2}$ [13], J and ρ are expected to be proportional to $\omega^{-1/2}$ for ideal microelectrode arrays. For high density arrays ($\theta \rightarrow 0$), the diffusion zones of adjacant active sites overlap extensively and, in the limit of total overlap of diffusion zones, the corresponding array electrodes have a virtually uniform diffusion-layer thickness across the face of the electrode and the current is proportional to $\omega^{1/2}$. Hence, for these high density array electrodes, J and ρ are expected to be independent of ω. These conclusions are consistent with predictions based on models which neglect the effect of radial mass transport [11, 12, 14]. For arrays of intermediate density ($0 \ll \theta \ll 1$), J and ρ are expected to be complex functions of $\omega^{1/2}$.

2. Experimental details

2.1. *Reagents*

All chemicals were reagent grade (Fisher) and water was purified in a Milli-Q system (Millipore) after passage through two D-45 deionizing tanks (Culligan). The solutions of 0.10 M H_2SO_4 were prepared by dilution of the concentrated reagent grade chemical (Mallinckrodt) in deionized water.

2.2. *Electrode fabrication*

The Pt–Ti_4O_7 composite materials were prepared by mixing the appropriate quantities of TiO_2 (Fisher), Ti_2O_3 (Johnson-Matthey) and Pt (Aldrich, 0.8–2.2 μm diam.). Each mixture was ground in an agate mortar until a uniform colour was obtained. Several drops of polyvinyl acetate (1% by volume) in ethanol were added to the mixture to produce a paste which was pressed into a cylindrical pellet (9 mm diam., 12 mm length) in a laboratory press (Carve) at a pressure of 3 ton cm^{-2}. Pelletization improved contact between particles and, thereby, increased diffusion rates during thermal processing.

The pellets were dried at 150 °C for 1 day and then placed in a tungsten Knudsen cell in an induction furnace. The temperature of the tungsten crucible was monitored using an optical pyrometer. The residual pressure in the furnace was lowered to below 10^{-5} torr using an oil diffusion pump backed by a mechanical pump. The temperature was then slowly increased to 800 °C and held constant for about 1 h to evaporate all traces of organic material. The temperature was then slowly increased to 1300 °C, under a vacuum of about 10^{-6} torr, and held constant for 5 h. Heating was terminated and the sample quenched by radiative heat loss in vacuum, allowing the sample to reach room temperature in about 2.5 h.

Disc electrodes were assembled by mounting thermally processed pellets into a metal socket at the end of a stainless steel shaft which could be inserted into the rotator assembly. Cylindrical surfaces of these pellets were coated with wax to prevent their contact with the aqueous test solutions and, furthermore, only the end (disc) surfaces were allowed to contact the test solutions.

Active surface areas (A_{act}) for Pt–Ti_4O_7 electrodes were calculated from the geometric areas (A_{geom}) and the volume fractions of Pt according to

$$A_{act} = [V_P/(V_T + V_P)]A_{geom} = (d_T/d_P)(M_P/M_T)(N_P/N_T)A_{geom} \quad (4)$$

where V, d, M and N represent the volume, density, molecule weight and number of moles, respectively; and the subscripts P and T designate Pt and Ti_4O_7, respectively.

2.3. *Surface characterization*

X-ray diffraction (XRD) data were obtained with an XDS-2000 (Scintag) diffractometer using CuK_{α_1} radiation. The sample was rotated during data collection to reduce effects of preferred orientation.

Micrographs and elemental analyses were obtained using a S-2460N scanning electron microscope (SEM, Hitachi) equipped with a LINK ISIS energy dispersive X-ray spectrometer (EDS, Oxford).

2.4. *Voltammetry*

Voltammetric data were obtained using a RDE4 potentiostat and AFMSRX rotator (Pine Instrument) interfaced with a 486 computer by a DT2800-A interface (Data Translation) using ASYST-3.1 software (Keithley, ASYST). The electrochemical cell was constructed from Pyrex with porous glass discs separating the working, reference and counter electrode

compartments. All potentials are reported in volts against a saturated calomel electrode (SCE, Fisher Scientific). The counter electrode was a coiled platinum wire (~7.6 cm^2).

The mass transport-limited current at a uniformly-accessible RDE (i.e., $A_{act}/A_{geom} = 1$) is a linear function of $\omega^{1/2}$, as indicated by the Levich equation [13]:

$$i = 0.62nFA_{geom}D^{2/3}\nu^{-1/6}\omega^{1/2}C^b \quad (5)$$

where A_{geom} is the geometric area (cm^2), ν is the solution kinematic viscosity ($cm^2\ s^{-1}$); and n, F and C^b have their usual electrochemical significance. For microelectrode arrays of low density ($A_{act}/A_{geom} \rightarrow 0$), that is, no overlap of adjacent diffusion zones, i is expected to be independent of $\omega^{1/2}$.

3. Results and discussion

3.1. *XRD and SEM data*

Figure 1(a) contains the XRD pattern for pure Pt metal [15]. Figure 1(b) contains the XRD pattern of Ti_4O_7 prepared by the method described but in the absence of Pt. This diffraction pattern is in good agreement with that reported for a single Ti_4O_7 crystal by Le Page and Marezie [16]. Figure 1(c)–(f) contains XRD patterns for Ti_4O_7 samples containing various amounts of Pt increasing from 0.1 to 5%. These patterns correspond exactly to combinations of the patterns in Figure 1(a) and (b) which indicates that these Pt-Ti_4O_7 samples correspond to heterogeneous

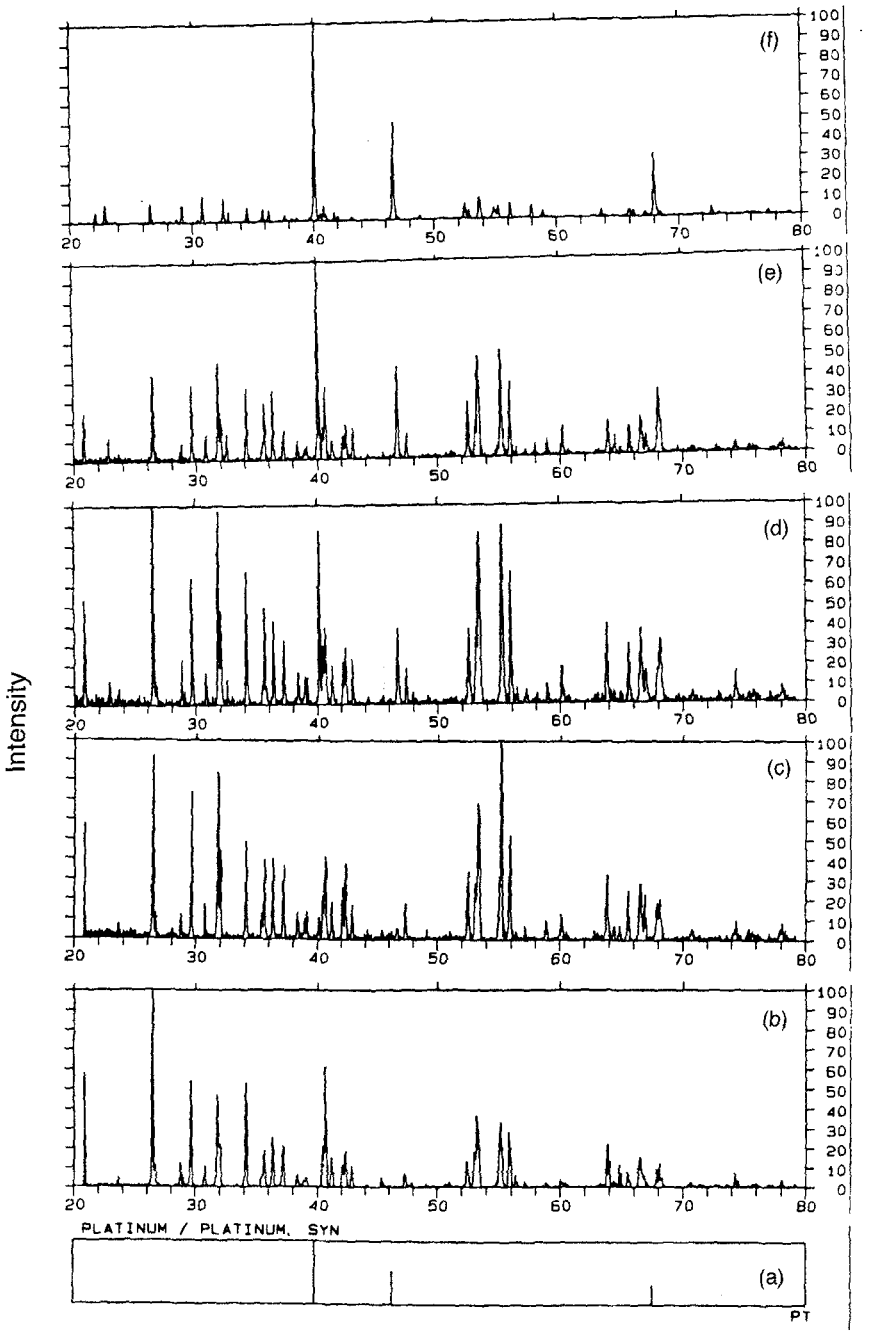

Fig. 1. X-ray powder diffraction patterns. Materials: (a) Pt, (b) Ti_4O_7, (c) 0.1% Pt-Ti_4O_7, (d) 0.5% Pt-Ti_4O_7, (e) 1% Pt-Ti_4O_7, (f) 5% Pt-Ti_4O_7.

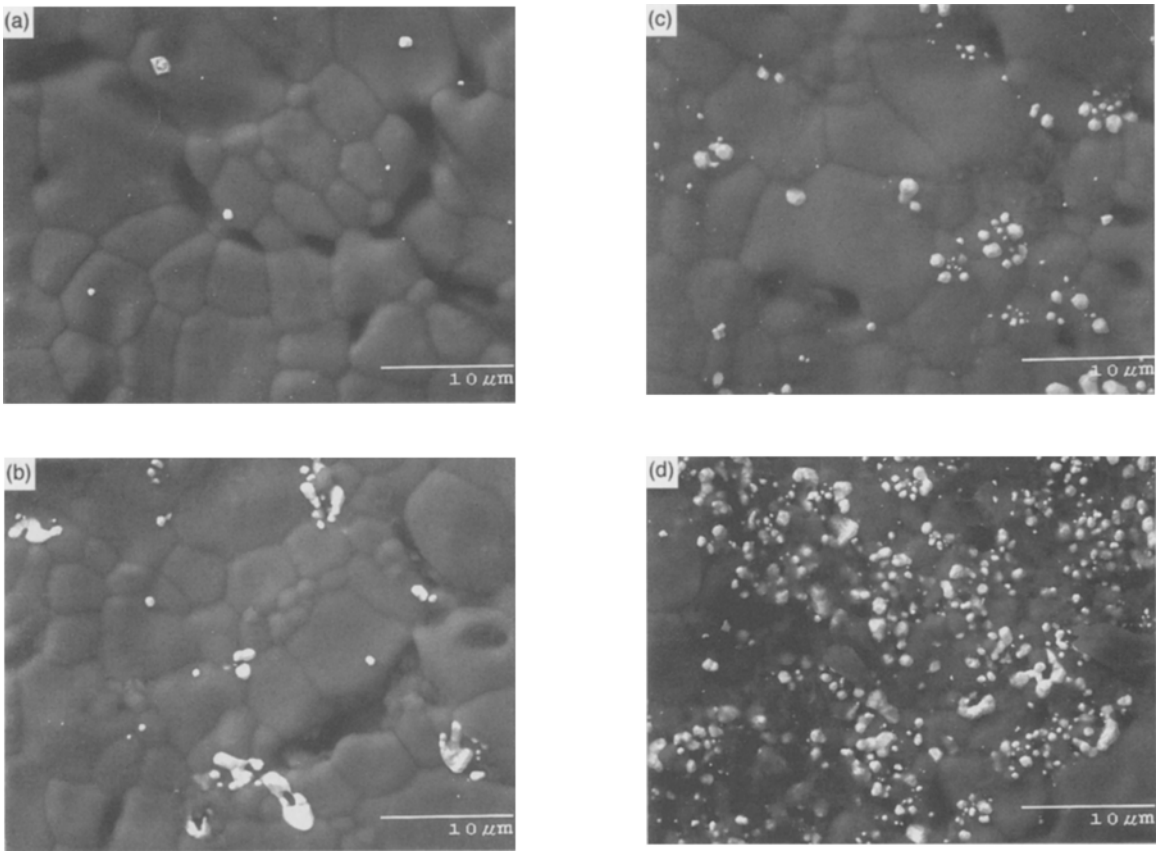

Fig. 2. Scanning electron micrographs of Pt–Ti_4O_7 electrode surfaces. (a) 0.1% Pt–Ti_4O_7, (b) 0.5% Pt–Ti_4O_7, (c) 1% Pt–Ti_4O_7, (d) 5% Pt–Ti_4O_7.

mixtures of pure Pt and Ti_4O_7. There is no evidence for the existence of a new intermetallic oxide. Hence, on this basis, it is expected that the Pt is distributed throughout the Ti_4O_7 matrices in the form of small metallic particles (i.e., microelectrodes). The average grain size in the samples was estimated on the basis of the Fresnel construction [17] to be on the order of 0.9 μm. Because the Fresnel calculation is weighted in favour of smaller particles, this result is considered to be consistent with the estimated size of the Pt particles (0.8 to 2.2 μm) used in the fabrication of these Pt–Ti_4O_7 materials.

Planar surfaces of Pt–Ti_4O_7 electrodes were examined using SEM and typical micrographs are shown in Fig. 2(a)–(d) as a function of increasing Pt content. During these experiments, the back scattering emission was detected to aid in the discrimination of the Pt particles from the Ti_4O_7 matrices and it is evident that the number of bright spots increases with increasing Pt content. The EDS spectra are shown in Fig. 3 for 0.1% Pt–Ti_4O_7 corresponding to (a) a dark region and (b) one of the bright spots in Fig. 2(a). It is apparent from these results that the bright spots in Fig. 2(a)–(d) correspond to Pt particles and there is no Pt in the Ti_4O_7 corresponding to the dark regions of these SEMs. The values of A_{act}/A_{geom} for the 1% Pt–Ti_4O_7 electrode was estimated from the SEM map to be within about 10% of the value calculated by Equation 4.

Platinum particles were determined to be quite stable in the Ti_4O_7 matrix and were not lost in significant amounts even when surfaces were subjected to mechanical polishing. Surfaces of the 0.1% Pt–Ti_4O_7 and 1% Pt–Ti_4O_7 electrodes were polished for several minutes using silicon carbide discs (LECO) with grit size increasing in the sequence 600-c, 800-c and 1200-c, using gentle pressure and water as lubricant. The micrographs for these electrodes were very similar to those shown in Fig. 2(a) and (c) for the unpolished surfaces. Furthermore, the percentage active areas of the polished 0.1% and 1% Pt–Ti_4O_7 surfaces were estimated from their respective SEM maps to be 0.12% and 0.99%, respectively. These values are very close to the expected values and are an indication of the stability of the Pt particles in the Pt–Ti_4O_7 surfaces even under the torturous treatment corresponding to mechanical polishing.

The average diameter for the Pt particles was estimated to be about 0.1 to 1 μm from SEM–EDS data, which is on the same order as the estimates from SEM data. It is apparent that the Pt particles are randomly rather than uniformly distributed within the Ti_4O_7 matrix. Hence, it also is evident that significant overlap can exist between the diffusion zones of some closely adjacent platinum microelectrodes, especially when the percentage of Pt is greater than 0.5%. The average distance between neighbouring Pt particles in the 0.1% Pt–Ti_4O_7 is about 8 μm and this material is expected to approach the behaviour of an ideal microelectrode array. The existence of porosity is evident in the SEM data for all Pt–Ti_4O_7 samples.

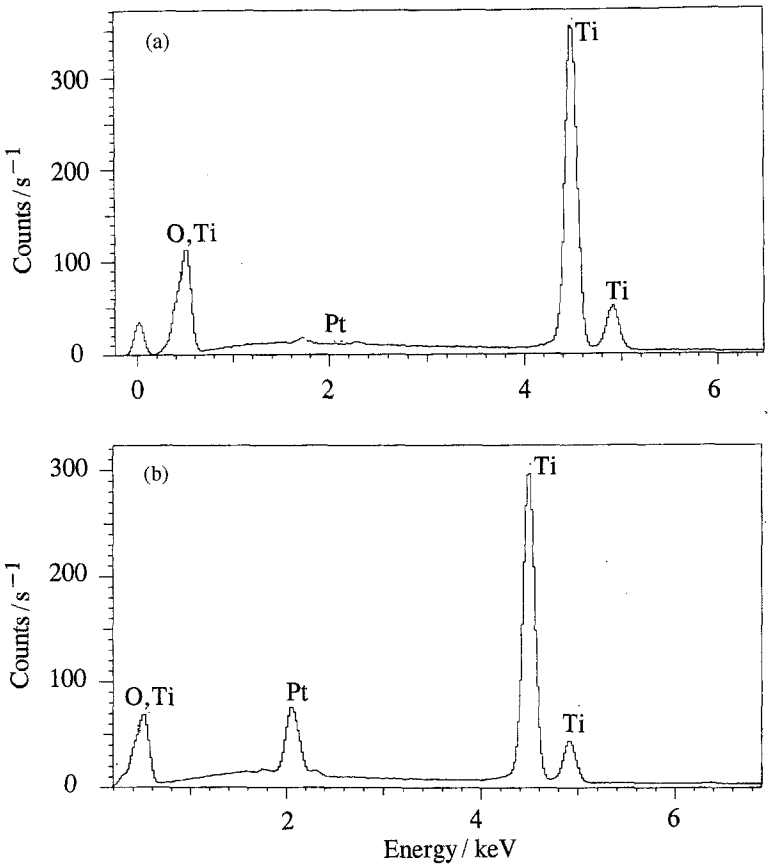

Fig. 3. EDS spectra for (a) a dark region and (b) one of the bright spots in the micrograph shown in Fig. 2(a).

3.2. *Background response*

Figure 4 shows the background current–potential (i/E) curves in deaerated 0.1 M H_2SO_4 for a Ti_4O_7 RDE ($A_{geom} = 0.74\,cm^2$) obtained in the potential region −0.35 to 2.8 V (curve (a)) and for the 1% Pt–Ti_4O_7 RDE ($A_{geom} = 0.74\,cm^2$) obtained in the region −0.35 to 1.6 V (curve (b)). The residual response for the Pt–Ti_4O_7 RDE is significantly different from that for the Ti_4O_7 RDE. Most obvious is the large difference in potentials for onset of rapid anodic breakdown of solvent with production of oxygen, i.e., ~1.2 V for the 1% Pt–Ti_4O_7 RDE compared with ~2.5 V for the Ti_4O_7 RDE. Double-layer charging is concluded to be responsible for the current observed at the Ti_4O_7 RDE throughout the region about −0.35 to 2.4 V and for the anodic current at the Pt–Ti_4O_7 RDE observed during the positive scan in the region about −0.3 to 0.4 V. Furthermore, for the Pt–Ti_4O_7 RDE, formation of surface oxide occurs at the Pt microelectrodes during the positive scan for $E > \sim 0.4$ V and this oxide is reduced during the negative scan to produce the cathodic peak in the region about 0.4 to −0.3 V with a peak potential at ~0.2 V. Any oxygen generated anodically at Pt microelectrodes within surface pores at $E > \sim 1.2$ V also can contribute to the cathodic current observed for $E < \sim 0.4$ V. These conclusions are consistent with the following observations: (i) the cathodic signal at 0.2 V did not vary with changes of rotational velocity in this deaerated solution; (ii) the cathodic signal at 0.2 V decreased when the scan limit of the preceding positive scan was decreased; and (iii) the cathodic signal at 0.2 V was proportional to the potential scan rate. Cathodic evolution of hydrogen occurs at the Pt microelectrodes in the Pt–Ti_4O_7 RDE for $E < -0.3$ V.

3.3. *Current responses for iodide*

Iodide was chosen as a model reactant for the voltammetric characterization of these electrode materials because oxidation of I^- to I_2 (1 equiv. mol^{-1}) occurs by a quasireversible process with $E_{1/2} = \sim 0.5$ V at Ru, Pt, Au, Ir and glassy carbon (GC) electrodes in

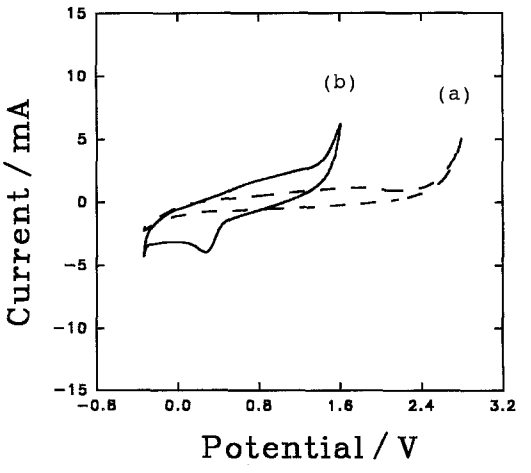

Fig. 4. Residual voltammetric response at Ti_4O_7 (curve (a)) and 1% Pt–Ti_4O_7 (curve (b)) rotated disc electrodes in 0.1 M H_2SO_4. Scan rate: 30 mV s^{-1}. Rotational velocity: 41.9 rad s^{-1}. Geometric area: 0.74 cm^2.

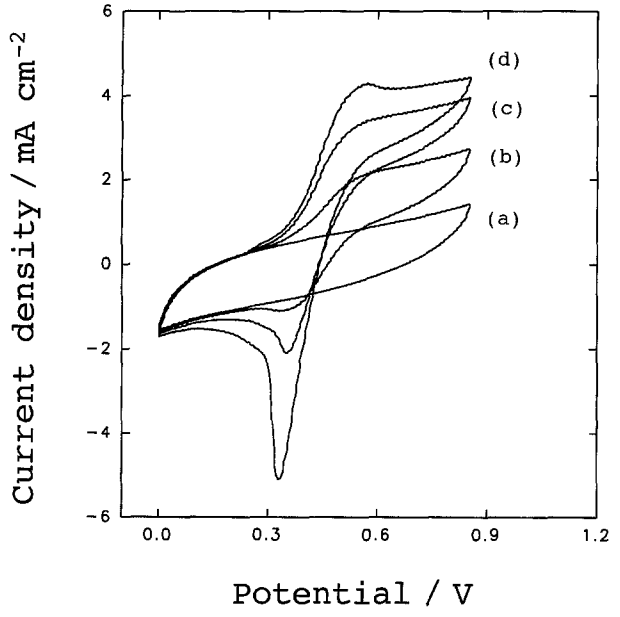

Fig. 5. Voltammetric response at the 3% Pt–Ti_4O_7 RDE as a function of I^- concentration in 0.10 M H_2SO_4. Concentration of I^- (mM): (a) 0, (b) 1.0, (c) 2.0, (d) 2.5. Rotational velocity: 41.9 rad s^{-1}. Scan rate: 30 mV s^{-1}.

acidic media [18, 19]. Voltammetric data are shown in Fig. 5 obtained using the 3% Pt–Ti_4O_7 RDE as a function of I^- concentration in 0.1 M H_2SO_4. A previous study demonstrated the total absence of reactivity of I^- at Ti_4O_7 electrodes [5]. Therefore, the anodic wave obtained during the positive scan with $E_{1/2} = \sim 0.45$ V is concluded to correspond to oxidation of I^- to I_2 at the Pt microelectrodes. The choice of 0.85 V for the positive scan limit in this experiment precluded the possibility for oxidation of I^- to IO_3^-. Cathodic peaks at ~0.35 V obtained during the negative scan are similar to peaks obtained at solid platinum electrodes (data not shown) and attributed to the cathodic stripping of I_2 adsorbed at the platinum surface. However, contribution to this

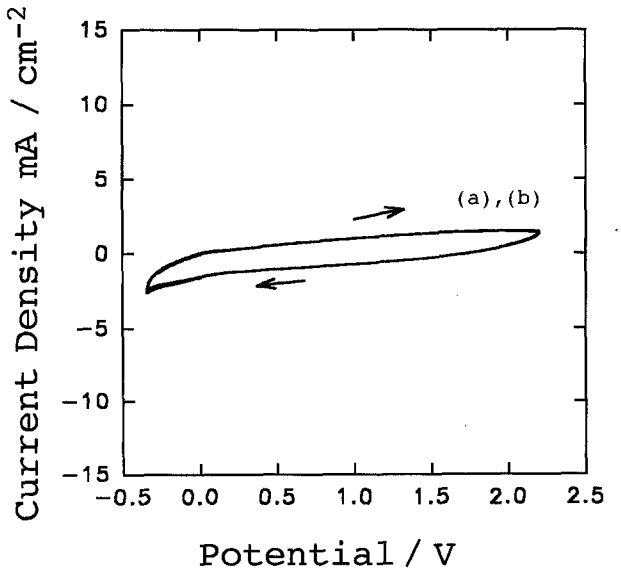

Fig. 6. Voltammetric data of Ti_4O_7 RDE without (curve (a)) and with (curve (b)) H_2O_2 (5 mM) at the potential range of −0.35 to 1.5 V in 0.1 M H_2SO_4. Scan rate: 30 mV s^{-1}. Rotational velocity: 41.9 rad s^{-1}.

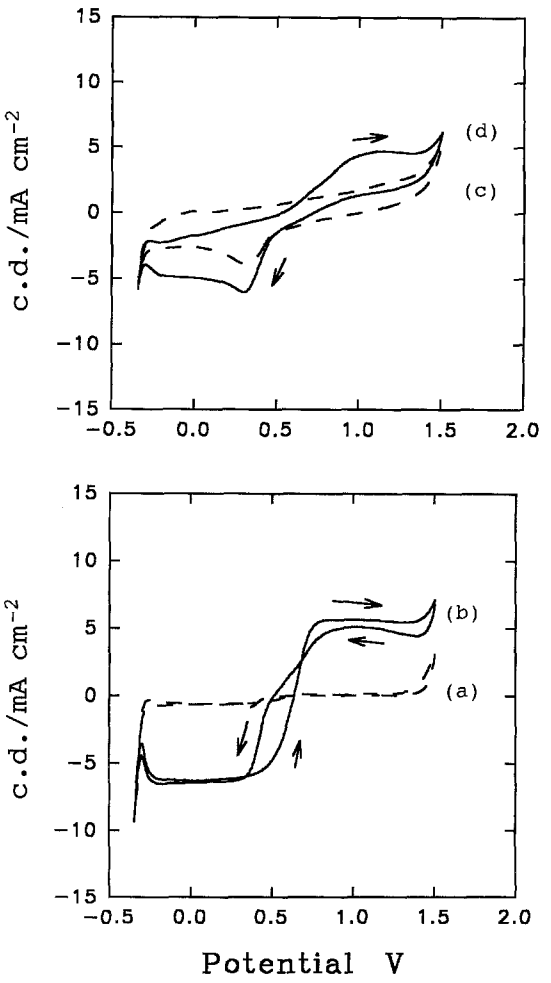

Fig. 7. Voltammetric response for H_2O_2 at Pt (lower curves) and 1% Pt–Ti_4O_7 (upper curves) rotated disc electrodes. Scan rate: 30 mV s^{-1}. Rotational velocity: 41.9 rad s^{-1}. Concentration of H_2O_2: (a, c) 0, (b, d) 3.0 mM.

cathodic peak for the Pt–Ti_4O_7 electrodes also is expected from cathodic reduction of I_2 trapped within surface pores.

3.4. *Current responses for hydrogen peroxide*

Hydrogen peroxide also was chosen as a reactant because both anodic and cathodic reactions having well-defined current plateaus are available for this compound at Pt electrode [20]. The anodic reaction corresponds to production of oxygen (2 equiv. mol^{-1}) and the cathodic reaction to production of water (2 equiv. mol^{-1}). Figure 6 contains voltammetric data obtained at the Ti_4O_7 RDE in 0.10 M H_2SO_4 without (curve (a)) and with (curve (b)) the presence of 5.0 mM H_2O_2 over the potential range −0.35 to 1.5 V. It is readily apparent that H_2O_2 is not electroactive at the Ti_4O_7 electrode and, therefore, this material is an ideally inert matrix for microelectrode arrays to be applied to oxidation and/or reduction of H_2O_2. It was reported by Baez *et al.* [21] that H_2O_2 can be reduced at Ti_4O_7 electrodes in acidic media only in the region $E < -0.8$ V.

Figure 7 (lower) contains voltammetric curves obtained at the Pt RDE and (upper) the 1% Pt–Ti_4O_7 RDE in the presence of 3 mM H_2O_2 (——).

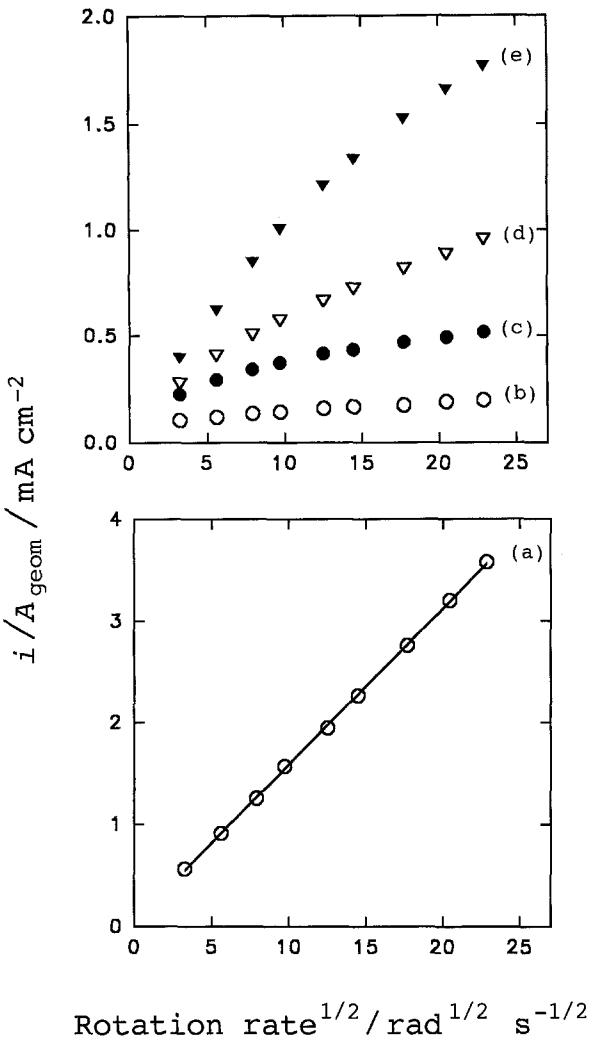

Fig. 8. Plots of apparent current density against square root of rotational velocity for various rotated disc electrodes for oxidation of I^- to I_2 at 0.70 V. Concentration of I^-: 0.5 mM. Electrodes: (a) Pt, (b) 0.1% Pt–Ti_4O_7, (c) 0.5% Pt–Ti_4O_7, (d) 1% Pt–Ti_4O_7, (e) 5% Pt–Ti_4O_7.

The background curves also are shown for comparison (– – –). The large background current obtained at the Pt–Ti_4O_7 RDE, corresponding primarily to double-layer charging, is concluded to be indicative of a high porosity for this electrode surface in comparison to the pure Pt RDE. The anodic waves corresponding to the positive scans in Fig. 7 (upper and lower) are concluded to correspond to the oxidation of H_2O_2 to O_2 at $E_{1/2} = \sim 0.60$ V for the Pt electrode (lower) and $E_{1/2} = \sim 0.80$ V for the 1% Pt–Ti_4O_7 electrode (upper). During the negative scan, the cathodic waves concluded to correspond to the reduction of H_2O_2 to H_2O are observed at $E_{1/2} = \sim 0.40$ V for Pt (lower) and $E_{1/2} = \sim 0.35$ V for 1% Pt–Ti_4O_7 (upper). These waves have well-defined current plateaus at the Pt RDE. The distorted appearance of the waves at the 1% Pt–Ti_4O_7 RDE results, at least in part, from the contribution of the large background current to the total voltammetric response and the contribution (peaked-shaped) from reaction of H_2O_2 contained within the surface pores.

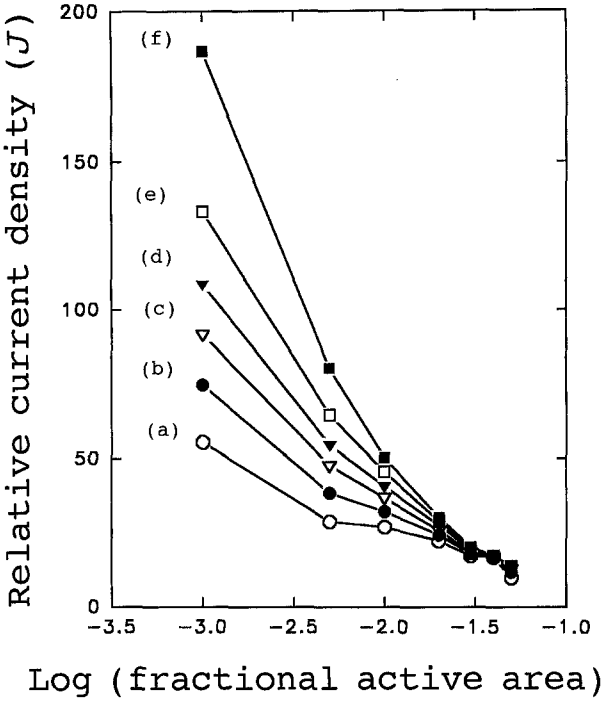

Fig. 9. Relative current density (J) as a function of fractional active area (A_{act}/A_{geom}) at Pt–Ti_4O_7 rotated disc electrodes for oxidation of I^- to I_2 at 0.70 V. Concentration of I^-: 0.5 mM. Rotational velocity: (a) 512, (b) 209, (c) 94.2, (d) 62.8, (e) 31.4 and (f) 10.5 rad s^{-1}.

3.5. *Comparison of current densities*

Figure 8 contains plots of current density (i/A_{geom}) against $\omega^{1/2}$ corresponding to the oxidation of I^- to I_2 at 0.70 V for the Pt (a), 0.1% Pt–Ti_4O_7 (b), 0.5% Pt–Ti_4O_7 (c), 1% Pt–Ti_4O_7 (d) and 5% Pt–Ti_4O_7 (e) RDEs. Curve (a) for the solid Pt electrode is linear ($r > 0.999$) with a near zero intercept which is indicative of a transport-limited reaction at a uniformly-accessible RDE (i.e. $A_{act}/A_{geom} = 1$). Values of i/A_{geom} observed for the 0.1% Pt–Ti_4O_7 RDE (b) are smaller than for the other Pt–Ti_4O_7 electrodes and also exhibit less dependence on rotational velocity. Zero dependence on rotational velocity is expected for ideal microelectrode arrays because of the absence of overlap between the diffusional zones for adjacent microelectrodes within the array. Hence, the 0.1% Pt–Ti_4O_7 electrode does not function as an ideal microelectrode array, undoubtedly because the Pt particles are not distributed uniformly within the electrode surface. The current responses for the other Pt–Ti_4O_7 electrodes represented in Fig. 8 are more complex, indicating significant overlap of the diffusional zones for adjacent microelectrodes, especially at low rotational velocities.

Figure 9 contains plots of relative current density (J) against $\log(A_{act}/A_{geom})$ as a function of rotational velocity for oxidation of I^- to I_2 at the Pt–Ti_4O_7 RDEs represented in Fig. 8. As a guide to the interpretation of these data, it is noted that $J = 1$ at all values of rotational velocity for a transport-limited reaction occurring at a solid RDE ($A_{act}/A_{geom} = 1$). It is apparent from Fig. 9 that the value of J increases for microelectrode arrays as the density of active sites is decreased

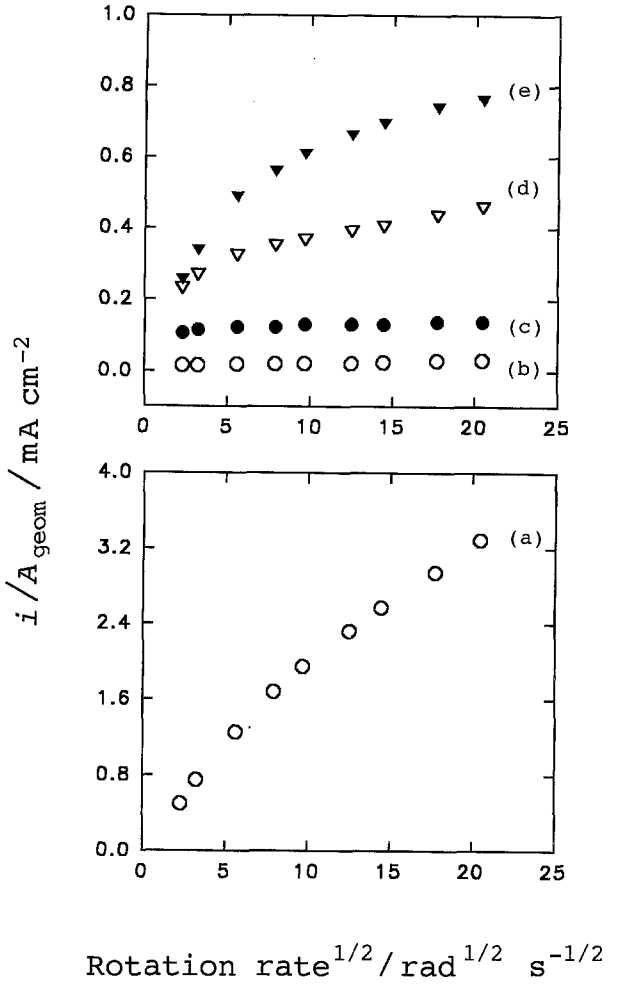

Fig. 10. Plots of apparent current density against square root of rotational velocity for various RDEs for oxidation of H_2O_2 to O_2 at 1.10 V. Concentration of H_2O_2: 0.5 mM. Electrodes: (a) Pt, (b) 0.1% Pt–Ti_4O_7, (c) 0.5% Pt–Ti_4O_7, (d) 1% Pt–Ti_4O_7 and (e) 5% Pt–Ti_4O_7.

and as rotational velocity is decreased. More specifically, the relative current density for the 0.1% Pt–Ti_4O_7 RDE is about 180 times larger than for the Pt RDE at a rotational velocity of 10.5 rad s^{-1}.

Figure 10 contains plots of i/A_{geom} against $\omega^{1/2}$ for the oxidation of H_2O_2 at 1.10 V for the solid Pt (a), 0.1% Pt–Ti_4O_7 (b), 0.5% Pt–Ti_4O_7 (c), 1% Pt–Ti_4O_7 (d) and 5% Pt–Ti_4O_7 (e) RDEs. This plot for a mass-transport limited current at a uniformly accessible RDE ($A_{act}/A_{geom} = 1$) is expected to be linear. Hence, the negative deviation in curve (a) is indicative of an electrode reaction under mixed control by the mass transport and electron-transfer processes. Figure 11 contains plots of J against $\log(A_{act}/A_{geom})$ as a function of rotational velocity for the oxidation of H_2O_2 to O_2 (1.10 V) at the various Pt–Ti_4O_7 RDEs represented in Fig. 10. As expected, J values increase as rotational velocity decreases. However, contrary to the trend demonstrated in Fig. 10, J values are at a maximum for the 1% Pt–Ti_4O_7 RDE and show a significant decline for electrodes with lower Pt content.

4. Conclusions

Platinum microarray electrodes can be fabricated using Ti_4O_7 as a conductive and electrochemically inert binder. The procedure is based on a conventional thermal process applied to a 2:1 mixture of TiO_2 and Ti_2O_3 powder with added Pt particles. Whereas this Pt–Ti_4O_7 product is porous, we suggest that these materials might be attractive for use in some large-scale electrolytic applications for which the cost of the precious metal must be minimized.

Of great significance is the observation that all of the Pt–Ti_4O_7 electrodes tested exhibit significantly enhanced levels of current density (i/A_{geom}), in comparison to a solid Pt electrode, which is expected for microarray electrodes. Furthermore, the dependence of amperometric response at these electrodes on increasing rotational velocity is diminished as the percentage of Pt is decreased. These observations are consistent with expectations for microarray electrodes

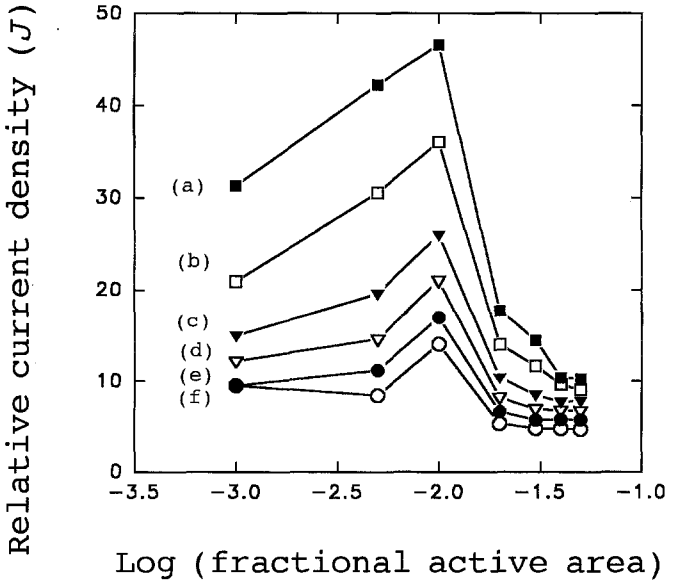

Fig. 11. Relative current density (J) as a function of fractional active area (A_{act}/A_{geom}) at Pt–Ti_4O_7 RDEs for oxidation of H_2O_2 to O_2 at 1.10 V. Concentration of H_2O_2: 0.5 mM. Rotational velocity: (a) 5.2, (b) 10.5, (c) 31.4, (d) 62.8, (e) 157 and (f) 418.9 rad s^{-1}.

[10, 12, 14, 22–25]. For the 1% $Pt-Ti_4O_7$ rotated disc electrode (RDE), the current enhancement factor (J), as defined by Equation 1, is 50 for oxidation of I^- to I_2 and 47 for oxidation of H_2O_2 to O_2 at a rotational velocity of 10.5 rad s^{-1}. For the 0.1% $Pt-Ti_4O_7$ RDE, J increases to 180 for oxidation of I^- but decreases to 30 for oxidation of H_2O_2 at 10.5 rad s^{-1}. An increase in J is expected for a decrease in Pt loading and we speculate that the decrease of J for H_2O_2 oxidation at the 0.1% $Pt-Ti_4O_7$ electrode is a consequence of slow heterogeneous kinetics which become significant in controlling the rate of the anodic process under conditions of high convective-diffusional flux (mol cm^{-2} s^{-1}).

The estimated steady-state diffusion layer thickness (δ) at an ideal microdisc electrode is $\pi r/4$, where r is the radius of the microdisc [26, 27]. Based on the average radius of $\sim 0.5\,\mu$m for Pt sites in the $Pt-Ti_4O_7$ RDEs prepared in this study, we estimate $\delta = 0.2\,\mu$m. This value of δ is significantly smaller than the value of 8 μm estimated for the average inter-site distance in the 0.1% $Pt-Ti_4O_7$ surfaces using SEM. Hence, from this comparison, it is logical to expect that adjacent diffusion zones will have minimal overlap for a microelectrode array of this composition if the Pt particles are uniformly distributed throughout.

Future research will seek to provide better control over porosity and distribution of Pt particles in the $Pt-Ti_4O_7$ materials prepared by this thermal technique. It is expected that porosity can be minimized by the use of smaller particle sizes for the starting materials and the increase of the packing density of the compacted mixture.

Acknowledgement

Ames Laboratory is operated for the US Department of Energy by Iowa State University under contract W-7405-ENG-82. This research was supported by the Director for Energy Research, Office of Basic Energy Sciences.

References

[1] S. L. Peterson and D. E. Tallman, *Anal. Chem.* **60** (1988) 82.
[2] D. J. Chesney, J. L. Anderson, D. E. Weissaar and D. E. Tallman, *Anal. Chim. Acta* **124** (1981) 321.
[3] J. E. Vitt, D. C. Johnson and D. E. Tallman, *Anal. Chem.* **65** (1993) 231.
[4] S. G. Weber, *ibid.* **61** (1989) 295.
[5] L. He, H. F. Franzen, J. E. Vitt and D. C. Johnson, *J. Electrochem. Soc.* **141** (1994) 1014.
[6] R. L. Clarke, *in* 'Proceedings of the Second International Forum on Electrolysis in the Chemical Industry' (edited by J. D. Genders and N. L. Weinberg), Deerfield Beach, FA (1988).
[7] P. C. S. Hayfield and R. L. Clarke, *in* 'Proceedings of the Electrochemical Society Meeting', Los Angeles, CA (1989).
[8] P. C. S. Hayfield, *US Patent 4 422 917* (1983).
[9] N. L. Weinberg, J. D. Genders and R. L. Clarke, *US Patent 4 936 970* (1990).
[10] F. Schelle, R. Landsberg and H. Wolf, *Electrochim. Acta* **15** (1970) 525.
[11] O. Contamin and E. J. Levart, *J. Electroanal. Chem.* **136** (1982) 259.
[12] E. Levart, *J. Electroanal. Chem.* **187** (1985) 247.
[13] V. G. Levich, 'Physicochemical Hydrodynamics', Prentice Hall, Englewood Cliffs, NJ (1962) p. 75.
[14] V. Yu. Filinovsky, *Electrochim. Acta* **25** (1980) 309.
[15] P. Villars and L. D. Calvert, 'Pearson's Handbook of Crystallographic Data for Intermetallic Phases', 2nd edn, ASM International, Materials Park, OH (1991) pp. 4776 and 5097.
[16] Y. Le Page and M. Marezie, *J. Solid State Chem.* **53** (1984) 13.
[17] A. Guinier, 'X-Ray Diffraction', W.H. Freeman & Co., San Francisco, CA and London (1963) p. 121.
[18] J. E. Vitt and D. C. Johnson, *J. Electrochem. Soc.* **138** (1992) 774.
[19] D. C. Johnson, *ibid.* **119** (1972) 331.
[20] V. G. Prabhu, L. R. Zarapkar and R. G. Dhaneshwar, *Electrochim. Acta* **26** (1981) 725.
[21] V. B. Baez, J. E. Grayes and D. Pletcher, *J. Electroanal. Chem.* **340** (1992) 273.
[22] R. Landsberg and R. Thiele, *Electrochim. Acta* **11** (1966) 1243.
[23] F. Schelle, S. Muller, R. Landsberg and H.-J. Spitzer, *J. Electroanal. Chem.* **19** (1968) 187.
[24] A. M. Trukhan, Yu. M. Povarov and P. D. Lukovtsev, *Elektrokhim.* **6** (1970) 425.
[25] *Idem, ibid.* **6** (1970) 602.
[26] K. B. Oldham, *J. Electroanal. Chem.* **122** (1981) 1.
[27] K. Aoki and J. G. Osteryoung, *ibid.* **122** (1981) 19.